Ball-lens Based Optical Add/Drop Multiplexers: Designs and Implementations

Wei Jiang[*a], Yingzhi Sun[a], Feng Zhao[a], Ray T. Chen[a], Baoping Guo[b], James Horwitz[b], and William Morey[b]
[a]Microelectronics Research Center, The University of Texas at Austin; [b]Radiant Photonics Inc.

ABSTRACT

A variety of ball-lens based optical add/drop multiplexers (OADMs) are designed and implemented. Insertion losses as low as 0.5 to 0.6 dB for the reflection light-path, and 1.2 to 1.5 dB for the transmission light-path are demonstrated. The 0.5-dB passband and –30 dB stopband for 100-GHz OADM are 0.35 nm and 1.15 nm, respectively. The reflection path has an isolation 15 dB. In addition to the distinct cost advantage of ball lenses over the GRIN lenses, the ball-lens based OADMs also offer a significant simplification in packaging due to the intrinsic spherical symmetry of ball lenses. Optical designs and optics-related packaging issues are discussed in detail.

Keywords: OADM, ball lens, WDM, packaging, RMS aberration spot size, thin film filter, TEC fiber, GRIN lens

1. INTRODUCTION

Wavelength-Division-Multiplexing (WDM) has been widely recognized as an enabling technology for high capacity optical networks. The optical add/drop multiplexers (OADM) are indispensable elements in WDM-based networks. Various approaches are considered in making such a device, including thin-film narrow bandpass filters, fiber Bragg gratings, arrayed waveguide gratings. Among these approaches, the one utilizing a thin film filter along with a pair of GRIN lenses has taken the lead due to its low cost, satisfactory performance, and high reliability.

GRIN-lens based devices have achieved considerable success in micro-optics due to the general perception about relative ease of the employment of GRIN lenses. However, a recent improvement in ball-lens coating technology[1] has aroused significant interest in expanding the usage of ball lenses in micro-optical devices. Now in many situations, ball lenses offer competitive performance and obvious convenience, while presenting a distinct cost advantage over GRIN lenses. In this paper, we present a few designs of ball-lens based OADMs, whose implementations were demonstrated to have competitive performance compared to the commercially available GRIN-lens based counterparts. The intrinsic symmetry of ball lenses also allows a significant simplification in packaging.

2. DESIGNS

2.1 Design Outline

In a beam-splitting ball lens proposed earlier [2], a thin-film beam-splitting filter is disposed at the mid-plane of a full-ball lens. The light is incident on the filter at 45° and is split into two beams traveling perpendicular to each other. A straightforward idea of OADM would be to replace the beam-splitter filter with a narrowband WDM filter. However, to our knowledge, no WDM filter working at 45° incident angle is available. And those narrowband filters intended to work at nearly normal incidence usually have very high transmission loss at large incident angles. Therefore, we design our first OADM (Design A) employing a similar setting, but the incident angle is nearly normal. The design is schematically shown in Fig. 1. The transmission light-path is between input and drop fibers, and the reflection light-path is between input and output fibers(when used as an add multiplexer, the light actually travels from drop to input fiber, and from output to input fiber for these paths). The ball lenses are made of SF2 glass and are 3.4 mm in diameter. The factors influencing the choice of glass and focal length will be discussed later. An ideal design would prefer the thin film filter to be deposited on the plano side of one of the half balls. Though not impossible, this substrate geometry is not compatible with mass production of filters. Therefore, we have used a standard thin-film filter having a substrate of 1 mm thick sandwiched between the two half balls. It turns out that the additional thickness of the filter substrate affects

[*] Corresponding author: jiang@ece.utexas.edu; phone 1 512 232-2586; fax 1 512 471-8575; Microelectronics Research Center, the University of Texas at Austin, 10100 Burnet Road, Building 160, Austin, TX USA 78758

only the angle of the drop fiber with the optical axis. Through aberration study, no significant degradation of performance is found due to the presence of a thick substrate. The fiber endfaces are located at the focal planes of the corresponding half balls. In this arrangement, a collimated beam is incident on the filter. The input and output fibers are fixed in two v-grooves on a metal strip. These two v-grooves are separated by *d* (center to center) at the end, and each is tilted at an angle θ_1 toward the optical axis. The drop fiber is at angle θ_2 with respect to the optical axis. The angles are given by

$$\theta_1 = \frac{d}{2(f+r)}, \qquad \theta_2 = \left[1 - \frac{n_a(n_a-1)}{r}\left(\frac{b}{n_b}+c\right)\right]\theta_1 . \tag{1}$$

where n_a and n_b are the refractive indices of the ball lenses and the filter substrate, respectively, *r* is the radius of curvature of the half-ball lenses, *f* the *front* focal length of the left half ball, *b* the thickness of the filter substrate and *c* the thickness of the thin air gap between the filter backside and the second ball lens. These relations are determined by paraxial raytracing. Note θ_1 is actually the angle of incidence (AOI) onto the thin film filter. The choice of fiber spacing *d* will affect AOI and therefore the center wavelength(CWL) shift of the filter passband. The major advantages of this system are the simplicity of packaging and mechanical stability due to the fact that lenses and filters are closely packed together.

However, it turns out the aberration of this system is large if single-mode fibers(SMFs) are to be used. Following Smith,[3] we study the image aberration of a single point on the object because the fiber core is much smaller than *h=d/2*, its distance from the optical axis. An indication of small aberration is that the image spot size of the center point of input fiber endface is considerably smaller than the fiber mode-field radius. In this case, even after appropriate defocusing, the root-mean-square(RMS) image spot radius is found to be larger than the SMF mode-field radius. We therefore introduce into this design the thermally-expanded-core (TEC) fibers, which have a larger mode field radius and a smaller NA. The RMS aberration spot radius increases with numerical aperture, while the TEC fiber mode field radius is approximately inversely proportional to the numerical aperture,[4] as shown in Fig. 2(a). One finds these two quantities cross at numerical aperture about 0.12 for typical lenses we used. Figure 2(b) shows the variation of the Strehl ratio[5] with NA. For NA less than 0.11, the central diffraction peak deduction due to aberration is less than 10% for both BK7 lenses and SF2 lenses. In experiments, we have used a TEC fiber with NA approximately 0.04 for Design A and C.

To further reduce the cost associated with TEC fibers, we develop Design B [Fig. 3(a)] where a pair of full ball lenses are used. The aberration study to be presented shows the aberrations in Design B is acceptable when standard SMF is used. For this system, there is not a natural center for the input and output fibers to aim at. Therefore, the fibers do not have to be tilted with respect to the axis. The airgaps *a* and *c* are determined through paraxial raytracing to be

$$a = f = \frac{(2-n_a)}{(n_a-1)}\frac{r}{2}, \qquad c = a - \frac{b}{n_b}, \tag{2}$$

where *f* is the front focal length of the ball lens, other symbols denote the same quantities as in Design A. The paraxial AOI onto the filter is

$$AOI = \frac{2h(n_a-1)}{n_a r}. \tag{3}$$

where *h* is the "object height", or the distance from the center of the input fiber endface to the optical axis.

Illustrated in Fig. 3 (b) is a comparative design of OADM using half-ball lenses in the parallel fiber setting. For this system, which we call Design C, the corresponding parameters are given by

$$a = \frac{r}{n_a(n_a - 1)},$$
$$c = a - \frac{b}{n_b}, \qquad (4)$$
$$AOI = (n_a - 1)\frac{h}{r}.$$

2.2 Aberration Study

For comparison, we will analyze the aberration for both full ball and half ball cases in the setting where the fibers are all parallel to the optical axis, i.e. Design B and C. Then we will show the fiber tilting in Design A does not introduce much difference in aberrations from Design C.

First, some commonalities of the aberrations in Design B and C are studied. Assume the axes of all three fibers are placed at a distance h from the optical axis and the light cones exiting the fibers have a half apex angle α. Since the object (the input fiber core) is much smaller than h, it is a convenient choice to pick the center ray of the light cone as the reference ray, and ray on the side of cone as the marginal ray. The aberration is essentially contributed by the spherical surfaces only. By raytracing one can easily show, in Designs B and C, when $c=a-b/n_b$ holds, there is a symmetry between the reflection and transmission light paths except for the region inside the filter substrate. Therefore, the aberration values are the same for the two "images" of the input fiber at the location of output and drop fibers. So the following aberration analysis applies to both output and drop fibers. A useful dimensionless parameter in evaluation of the aberration is q, as we call. For Design B and C, it is defined as

$$q_B = \frac{2h(n_a - 1)}{\alpha n_a r},$$
$$q_C = \frac{h}{\alpha r}(n_a - 1), \qquad (5)$$

respectively. For h=62.5 μm, NA=0.14 and n_a=1.50065(BK7), r=1.35 mm, one finds q_B=0.22 and q_C=0.16. For values of q small compared to unity, we can show that the contribution of astigmatism and Petzval to the aberration are all approximately q^2 times smaller than the spherical aberration, the distortion is q^3 times smaller than the spherical aberration. The sagittal coma on each surface is approximately q times smaller than the spherical aberration. However, sagittal comas on symmetrical pairs of spherical surfaces tend to have opposite sign and cancel each other, leaving the leading term in the total coma of order q^2. Note all spherical surfaces contributes to the spherical aberration with a consistent sign. Therefore, in this system, the spherical aberration is the major concern.

The following semi-quantitative analysis shows that generally design B has significantly lower aberration than Design C. We assume the fiber NA, material and radius of the lenses are same in both designs. According to aberration theory, the transverse spherical aberration TSC of a surface is given by[3]

$$TSC = C_1(u' + i)yi^2h \qquad (6)$$

where C_1 is a constant same for same kind of surfaces in two systems, h is the final image height, i is the incident angle of the marginal ray on the surface, u' is the marginal ray slope after refraction and y is the height at which the marginal ray intersects the current surface. The angle i for the half ball system per surface on average is about twice larger than the corresponding value in the full ball system. The ray height y at each spherical surface is always smaller in Design B than in Design C. Particularly, it scales roughly linearly with the front/back focal length for the first/last surface. Note the front focal length of the half ball is about quadruple of that of the full ball (for index around 1.5). The remaining factor in Eq. (6), for most surfaces, yields higher values in half ball case also. Now consider we have half number of spherical surfaces in Design C compared to Design B, we reach the estimate that the spherical aberration is 8 times or more in Design C compared to Design B. The results from rigorous Seidel aberration calculation are shown in Table 1. Note the spherical aberration, by convention, refers to its value at paraxial image plane, while the RMS spot radius listed

is its minimum value along the optical axis, see Appendix. For both types of lenses listed, the ratios of corresponding aberrations between the Design C and B are around 10.

In addition, it turns out that we do not need to do a separate aberration analysis for Design A. By properly tilting the local coordinate systems on each surfaces in Design C, one can prove that Design A has essentially the same aberration as a special case Design C where h=0. We also note he aberration only weakly depends on h for h below 250 μm.

2.3 Choice of Components

One design aspect we have not discussed until this point is the selection of glass material and the radius of the ball lenses. To lower the cost, we use the common materials such as BK7 and SF2, which are inexpensive but have low refractive indices. The use of a material having higher refractive index reduces the aberration further, but usually incurs higher cost for materials. Since the full ball Design B has demonstrated low enough insertion loss, we have not proceeded to using materials other than BK7 for that design. The choice of the radius of the ball lenses needs to take into account the focal length and filter incident angle requirement from the optical design, the size of fiber ferrules, and total package size. It is found that for refractive index of ball lens around 1.5 and h=62.5 μm, the radius of the ball should be around 2.7 mm to yield the common 1.8° incident angle on the filter in Design B. For half ball designs, the filter AOIs are in the range of 0.8 to 2.6 degrees, depending on h. Such a deviation from 1.8 degree introduces an extra shift in the central wavelength of the filter passband, and possibly a slight change in transmission loss, while leaving all other parameters unchanged.

2.4 Packaging Considerations

A considerably simplified packaging scheme are designed for these systems. The general idea is to first package lenses and filters together into a lens set without alignment. Then the fibers, or fiber ferrules (or holders), are aligned to the lens set. In a typical GRIN-lens based OADM, there are three alignment steps. They are (1)between a dual-fiber ferrule and one GRIN lens, (2) between a drop fiber ferrule and the other GRIN lens, and (3) between the two GRIN lenses. Our packaging scheme of ball-lens based OADMs allows the omission of the alignment procedure between lenses and filter, therefore saves a lot in alignment work compared to a GRIN-lens based OADM.

The viability of this packaging scheme is supported by several optical and mechanical considerations. The misalignments within the lens set has two effects: the change of the image position and orientation in space and the increase of the aberration. The first type of effect can always be compensated by moving the receiving fibers. For example, in Design C, the tilt of the filter results in a change of image position Δy at the output fiber, one can move the dual fiber ferrule holding input and output by $\Delta y/2$ to compensate this change. For the image at the drop fiber, the movement is straightforward. For various such compensations, the movement range is around a few dozens of microns. For the aberration increase due to misalignment, two attributes greatly simplify the analysis (1) the intrinsic symmetry of half and full balls; (2) the extremely weak dependence of aberration on airgap thickness. By these two attributes, significant aberration increases in all designs come only from the lateral misalignment of axes of the two lenses. Although, in Design C, the tilt of half ball may produce some small aberration increase also. All other misalignments are either geometrically equivalent to the above two types, or have negligible effects on aberration. The aberration increases due to misalignments are illustrated in Fig. 4 and 5 for Design B and C. For Design C, note the TEC fibers have core size around 35 μm. Therefore a lateral misalignment below 0.1 mm does not result in an unacceptable loss according to Fig. 5(d). For Design A, the misalignments have similar effects as for Design C, except we do not need to consider the tilts of half balls.

The above compensational movements and the refocusing movement demands that the packaging design leaves enough space (usually in the range of 0.1 um) during the alignment. On the other hand, epoxy application desires minimal spacing between parts to reduce the alignment shift after curing. This duality presents one major challenge in packaging, particularly due to the tight loss margin of OADMs. In our designs, small extra parts are used to fill in the position to reduce the space. To fit for all possibilities of space geometry after alignment demands thoughtful shape design of these parts. Combined with careful packaging labor, we can achieve a loss increase of less than 0.1 dB after epoxy curing.

3. RESULTS AND DISCUSSIONS

3.1 Comparison of Raw Filter Data and Packaged Device

We compare some critical performance parameters after packaging with the original filter data. A 200-GHz OADM of design B using a pair of BK7 2.5-mm-diameter ball lenses is analyzed in Table 2. The "Raw Filter" data were provided with the filter and were measured at normal incidence. The spectra of transmission and reflection light-paths are presented in Fig. 6 for all three designs. The picture of a packaged OADM is shown in Fig. 7. Table 2 shows a slight reduction of the 0.5-dB bandwidth after packaging. However, it is still much higher than 0.5 nm, typical requirement of a 200-GHz OADM. The peak insertion loss is 1.26 dB. A more careful and stricter consideration of transmission bandwidth of this device needs to take into account the isolation capability of the reflection light-path. Figure 6(b) shows that from 1548.84 nm to 1549.54 nm, the reflection path isolation is better than 16dB, a typical value of GRIN-lens OADM. The transmission path has its insertion loss less than 1.58 dB over this spectral width of 0.7 nm. The stopband increases slightly. The change of ripple is below detection. Polarization dependent loss (PDL) is less than 0.25 dB.

The shift of center wavelength is expected. An ideal design B would require a 2.7-mm-diameter ball lens to produce the typical 1.8° AOI, at which the filter may have a center wavelength shift of approximately 0.3 nm. Due to the unavailability of 2.7-mm ball lens, we substituted a 2.5-mm-diameter, which should produce an AOI of 1.91° by Eq. (3). The relation between the CWL shift and tilted angle is given by[6]

$$\frac{\Delta\lambda}{\lambda_0} = \frac{\theta_i^2}{2n^{*2}} \qquad (7)$$

where λ_0 is the central wavelength of the filter at zero AOI, $\Delta\lambda$ is the CWL shift at incident angle θ_i, and n^* is the effective refractive index of the dielectric stack. Using this relation, the expected CWL shift is 0.34 nm for the designed 1.91° AOI. Using the relation reversely, the actual 0.43 nm wavelength shift is found to correspond to 2.15° incident angle. Though the universal equation (7) may not be accurate due to variations in filtering production, we can *estimate* from our data that usually the angular misalignments are less than quarter degrees. The slight bandwidth change is in accordance with narrow band theory[6], which predicts it is of the order θ_i^4.

3.2 Comparison of measured performances and packaging issues of different designs

We compare the performance of various designs in Fig. 6 and Table 3. For design A, from 1550.31 nm to 1550.90 nm, the transmission path has insertion loss less than 1.87 dB (note the peak insertion loss for this path is 1.51 dB). The reflection path has isolation greater than 15 dB for this wavelength range. This range is about 0.1 nm narrower than the data for Design B presented above because the filters used for Design A and C have 0.5 dB bandwidth about 0.1 nm(at normal incidence) narrower than the filter used in Design B. For Design C, from 1550.69 nm to 1551.27 nm, the insertion loss for transmission path is less than 3.4 dB (peak at 2.78 dB), and isolation of reflection path is greater than 14 dB. The 30-dB stopband of transmission path is around 2.42 nm for both cases. Ripple and PDL are both less than 0.25 dB. Design A and C were implemented using uncoated half-ball lenses and TEC fibers. The half-ball lenses are made up of SF2 glass and 3.4 mm in diameter. The expected losses are presented in parentheses in Table 3 after deducting the excess losses due to reflection. Note for SF2 lens used in half-ball designs, the reflection loss in air is around 0.25 dB per surface. The reflection loss per fiber endface is estimated to be 0.15 dB. Each light path in Design C has 4 uncoated lens surfaces and 2 uncoated fiber endfaces, which corresponds to a total of 1.3 dB excess loss. In Design A, the filter front surface is in contact with the plano surface of one half-ball lens and the coating was designed to roughly index-matched to SF2. Therefore, we have deducted reflection losses of 0.8 dB for reflection path and 1.05 dB for transmission path. (Since no AR coating are perfect, we leave about 0.1 dB margin for reflection loss in Table 3).

We look at Design A first. A major advantage of this design is that the dual v-groove does not need micron precision for the separation of the input and output fibers. Figure 8 shows microscopic v-groove pictures with and without fibers therein. Because the v-grooves have an angle with respect to each other, the fibers can be slid in the v-grooves to compensate for an error in the fiber end lateral separation over a range of 50 μm. Therefore, it saves cost to use the metal v-groove compared to precision fiber ferrules. Another advantage of the system is the mechanical stability of the system. In Design A, only one spacer ring is placed between two half-ball lenses for separation, while the filter is directly affixed to one of the half ball. In comparison, in Design C, two half-ball lenses are separated by a pair of spacer rings with a filter sandwiched in between. Due to the three intermediate elements, the angular alignment between left and right half balls is generally worse in Design C than in Design A. This is one of the factors explaining why Design A has a transmission-path insertion loss much better than Design C. The ferrules used in Design C separate fibers at 250 μm, corresponding to an object height of 125 μm, while in Design A the equivalent object height is zero. The higher the

object height, the more the aberration. Another important source of extra loss in Design C is that the TEC fibers may suffer some damage when they were put into the ferrules. Since the TEC fibers are weakened in structure due to the extra thermal process,[7] this type of damage easily occurs and may give fairly large losses(In Design A, the v-grooves holding the fibers are open-structures). We did not investigate this factor in depth since Design C is studied only for comparative purpose.

However, comparing the figures after deducting reflection losses, the reflection path in Design A has a slightly higher insertion loss than that in Design C. This can be explained as follows. In Design A, we used low precision metal v-grooves to hold the input and output fibers, as shown in Fig. 9 (a). If the separation of center line of v-grooves is $d+\Delta d$ (in actual machining, a pre-offset is added to make sure Δd always positive) at the edge of the metal strip, we can slide the input and output fibers outward until the centers of their endfaces are separated by d. However, due to the resolution and measurement limitation of the microscope that can be used with the alignment process, it is difficult to fix the separation d to an accuracy below 5 μm (note TEC fiber core size is 35 μm). Thus a moderate extra loss occurs. If we use SMF, we can always convert such translational misalignment into angular misalignment. In Fig. 9 (b), we illustrate such a situation. Ideally, the fibers are separated by d, and tilted at an angle θ_1. If the actual separation is $d-\Delta d$(Δd can be positive or negative), one can rotate the metal strip holding two fibers counterclockwise by an angle $\Delta\theta$, which can be computed from Δd by differentiating Eq. (1). The rotation should centered around the end of upper fiber. Then the lower fiber solely has an angular misalignment of $2\Delta\theta$, with a negligible translational misalignment. For Δd =3 μm, one can estimate $\Delta\theta$ is about 0.03°, which is much smaller than the NA angle of a SMF. Drop fiber does not suffer from such a problem because its location relative to the input fiber is not constrained by the v-grooves.

Comparing various designs in Table 3, it is obvious that Design B has significantly better optical performance compared to Design C. Although compared to Design A, it needs precision ferrules and 2 spacer rings between filters and ball lenses. These add to the cost and the packaging complexity. If furnished with better alignment tools and AR coated lenses, Design A can yield best results with an extremely low insertion in both paths. But it needs TEC fibers. We should point out that it is possible to produce an optical design for a full-ball lens OADM with SMF fibers titled with respect to the axis. And the previous discussion clarifies the solution to the misalignment problem of using tilted v-grooves to hold SMF fibers. Therefore, this design will eliminate the costs of TEC fibers in Design A and precision fiber ferrules in Design B. The performance is expected to be comparable to Design B. There will a few packaging issues associated with the open structure of fibers holders. Also, one may need to do custom AR coating for fibers held in v-grooves.

3.3 100-GHz OADM

Due to the limited availability of 100 GHz WDM filters, most of our comparative experiments are conducted using 200 GHz filters. Experiments on 100 GHz OADMs are done for Design B only. The spectra for reflection and transmission paths are presented in Fig. 10. The 0.5-dB bandwidth is about 0.35 nm. The peak insertion losses are 0.54 dB and 1.44 dB for reflection and transmission paths, respectively. The 30 dB stopband width is 1.15 nm for the transmission path. From 1555.80 nm to 1556.14 nm, the isolation of reflection path is better than 15 dB. PDL and ripple are less than 0.25 dB.

4. CONCLUSION

We have studied a variety of designs and implementations of ball-lens based OADMs. At a lower cost, the ball-lens based OADMs are demonstrated to have competitive performance compared to GRIN-lens based OADMs. The ball-lens based OADMs also save one third of the alignment work in packaging. Among various designs, Design A does not need micron precision ferrule and is mechanically simple and stable, but needs TEC fibers. Design B has lower aberration under the same conditions and does not need TEC fibers, but needs precision ferrules.

5. APPENDIX: DEFOCUS AND RMS SPOT SIZE FOR SEIDEL ABERRATIONS

Root-mean-square spot radius is used in this paper because it usually yields a better estimate of actual spot size compared to the spot radius given simply by the transverse aberration of the marginal rays. Consider an on-axis point. When the third order aberration is dominant in a uncorrected positive lens, the marginal rays focus at a point closer to the lens than the paraxial focus. We can assume that the rays exiting the lens at an angle θ with respect to the optical axis focus at $z=f(\theta)$. For convenience, we choose the paraxial focus to be the origin of z axis, therefore, $f(0)=0$. For a system dominated by third order aberration, $f(\theta)=-A\,\theta^2$, where A is a constant. For simplicity, we always take the sign of θ to be

positive in this part of calculation. Suppose an image plane is placed at *z*. To the accuracy of third order, a ray exiting the lens at an angle θ strikes this plane at the radius

$$r(z,\theta) = \left| [z - f(\theta)]\theta \right|. \quad \text{(A1)}$$

For a system with small image NA and reasonable third order aberration, the exit pupil has an area element $dA_e = f_0^2 \theta d\theta d\varphi$, where φ is the azimuthal angle and f_0 is the focal length of the lens. To the accuracy of third order, the root-mean-square spot size can be evaluated

$$r_{rms}^2(z) = \frac{\int_0^\alpha r^2(z,\theta) dA_e}{\int_0^\alpha dA_e} = \tfrac{1}{2}\alpha^2 z^2 + \tfrac{2}{3} A\alpha^4 z + \tfrac{1}{4} A^2 \alpha^6. \quad \text{(A2)}$$

The minimum RMS spot size is found to be $\frac{1}{6} A\alpha^3$, when the image plane is located at $z = -\frac{2}{3} A\alpha^2$. These results are slightly different from those obtained by measuring a spot through the maximum aberration[3]. Note the absolute value of the transverse and longitudinal aberration for marginal rays are $A\alpha^3$ and $A\alpha^2$, respectively. The RMS spot size at the paraxial focus is half of the transverse aberration of marginal rays, which is obtained by evaluating Eq. (A2) at $z=0$. By defocusing about two thirds of the longitudinal aberration, the RMS spot size is reduced 3 times. The above analysis is valid also for $h << f \bullet NA$.

ACKNOLEDGEMENTS

The authors thank Dr. Jie Qiao, Dr. Xuegong Deng, Chengxin Yang for many helpful discussions. Also many thanks to Ray Collins for constant assistance in the laboratory.

REFERENCES

1. T. Clark and K. Wanser, "Ball vs. gradient index lenses," *Photonics Spectra,* **Feb.** pp. 94-96, 2001.
2. J. Ai, J. Popelek, Y. Li, and R. T. Chen, "Beam-splitting ball lens: a new integrated optical component," *Opt. Lett.*, **24**, pp. 1478-1480, 1999.
3. W. J. Smith, *Modern Optical Engineering,* pp. 301-366, McGraw-Hill, New York, 2000.
4. Tohihiro Orito, SOCC Optoelectronics (USA), Inc., personal communication, 2000.
5. E.L. O'Neill, *Introduction to Statistical Optics,* pp. 88, Addison-Wesley, Reading, Massachusettes, 1963.
6. H. A. Macleod, *Thin-Film Optical Filters,* 2nd ed., McGraw-Hill, New York, 1989.
7. K. Shiraishi, Y. Aizawa, and S. Kawakami, "Beam expanding fiber using thermal diffusion of the dopant**,"** *J. Lightwave Tech.*, **8**, pp. 1151-1161, 1990.

TABLES

Table 1. Aberration comparison of different designs (Unit: micron)

Glass, Diameter	BK7, 2.7 mm		SF2, 3.4mm	
	Spherical Aberration	RMS spot radius	Spherical Aberration	RMS spot radius
Full Ball	7.1	1.18	5.04	0.84
Half Ball	69.1	11.5	53.1	8.85

Table 2. Comparison of packaged device and raw filter data.

	CWL (3dB average) (nm)	Bandwidth @0.5dB (nm)	Transmission Peak Loss (dB)	Stopband @30dB (nm)	Ripple (dB)
Raw Filter	1549.63	0.86	0.39	2.24	0.12 ~ 0.22
Device	1549.20	0.80	1.26	2.41	<0.2

Table 3. Peak Insertion Loss of different designs (200 GHz) (Unit: dB)

Design	A	B	C
Reflection path	2.1 (1.4)*	0.5	2.3 (1.1)
Transmission path	1.5 (0.6)	1.26	2.8 (1.6)

*Expected insertion losses after deducting reflection loss are presented in parentheses, for Design A and C.

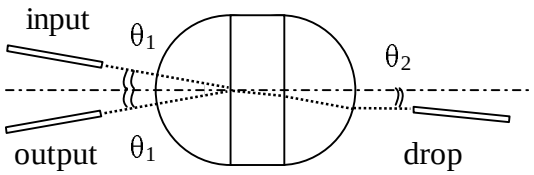

Fig. 1. A half-ball OADM with tilted fibers (Design A).

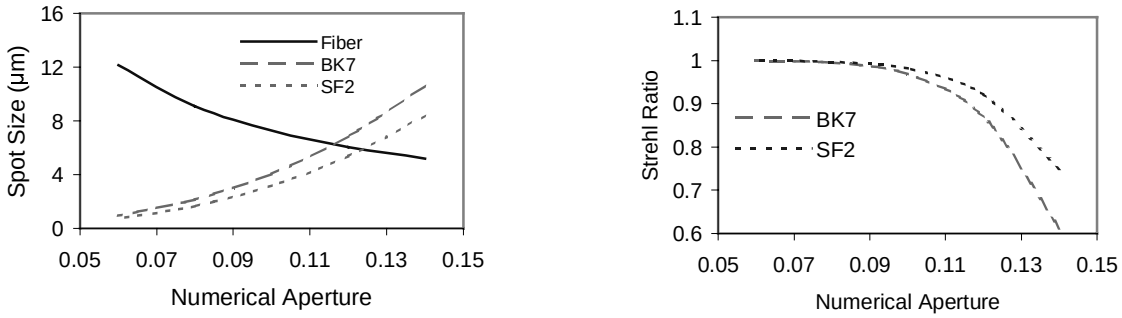

Fig. 2 Effect of NA reduction: (a) RMS Aberration spot radius and fiber mode-field radius vs. NA. (b) Change of Strehl ratio.

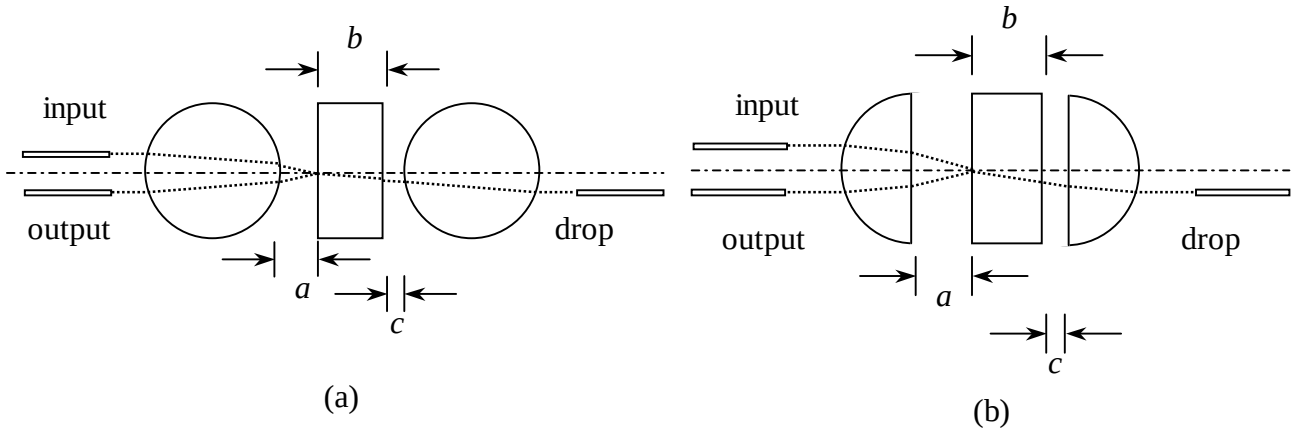

Fig. 3 (a) Full-ball lens OADM (Design B). (b) Half-ball lens OADM with parallel fibers (Design C).

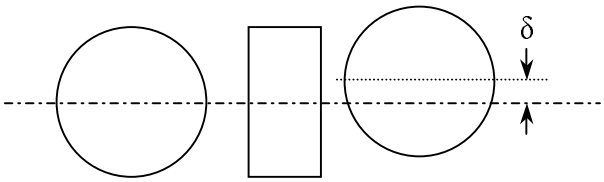

(a)

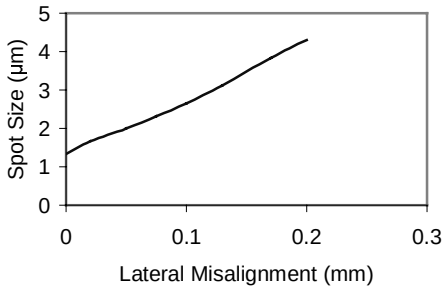

(b)

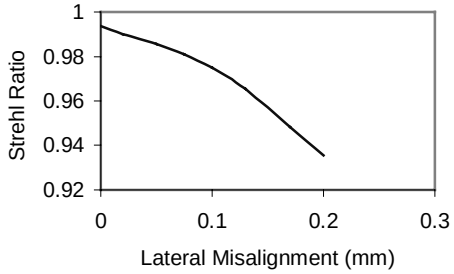

(c)

Fig. 4 (a) Illustration of misalignment in Design B. (b) The spot size change due to such misalignment. (c) Change of Strehl ratio

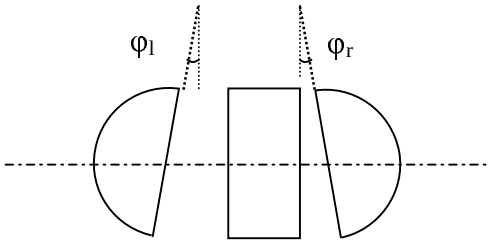

(a)

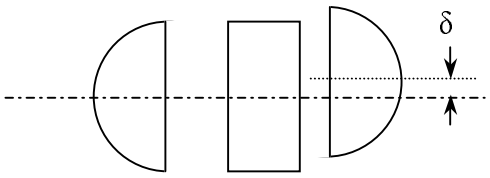

(b)

Fig. 5 Misalignments in Design C and accompanying aberration increases. (a) Non-parallelism between the filter surface and the plano surfaces of the half-balls. (b) Lateral separation between the axes of two half-balls. The changes of transverse aberration with (c) angular misalignment, (d) with lateral misalignment.

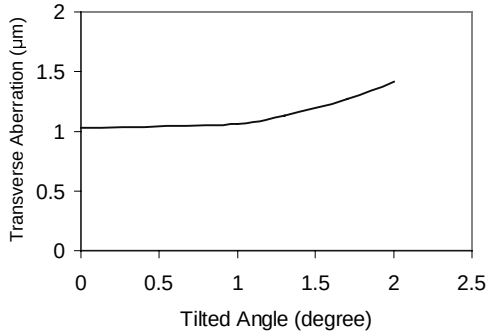

(c)

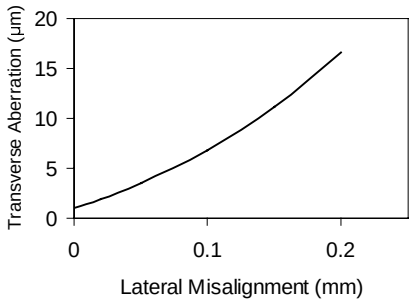

(d)

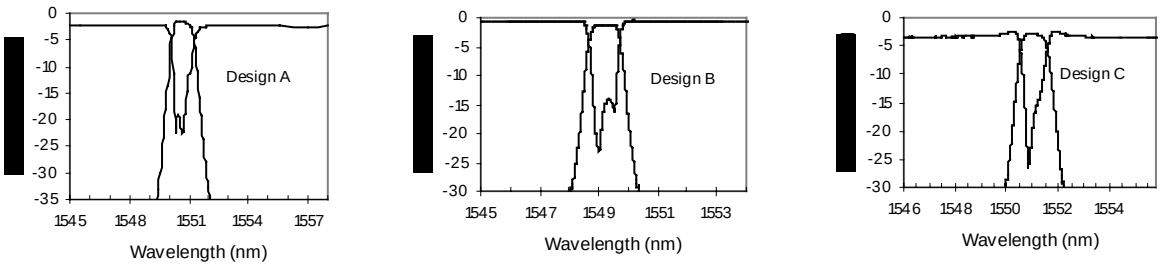

(a) (b) (c)

Fig. 6 Comparison of different designs of 200-GHz OADM. (a) Design A; (b) Design B; (c) Design C.

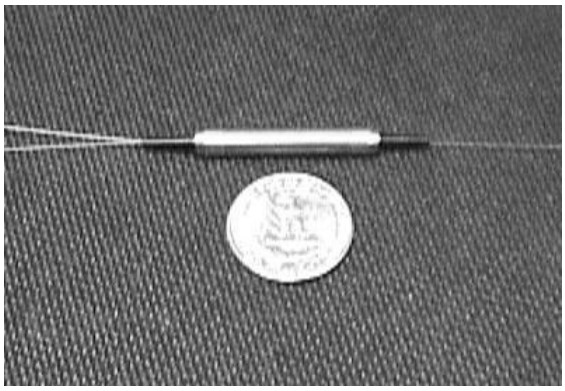

Fig. 7 A packaged 200-GHz OADM (Design B), along with a quarter dollar coin for a sense of size.

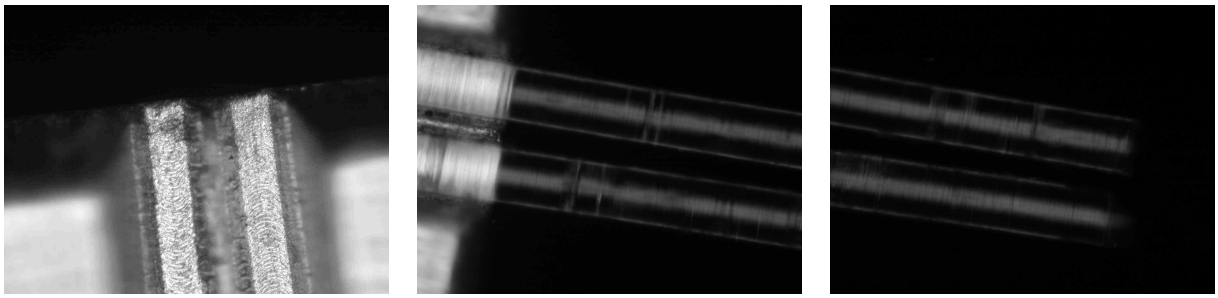

(a) (b) (c)

Fig. 8 The microscopic pictures of v-grooves in Design A. (a) v-grooves only, (b) v-grooves with fibers in it, (c) fiber ends.

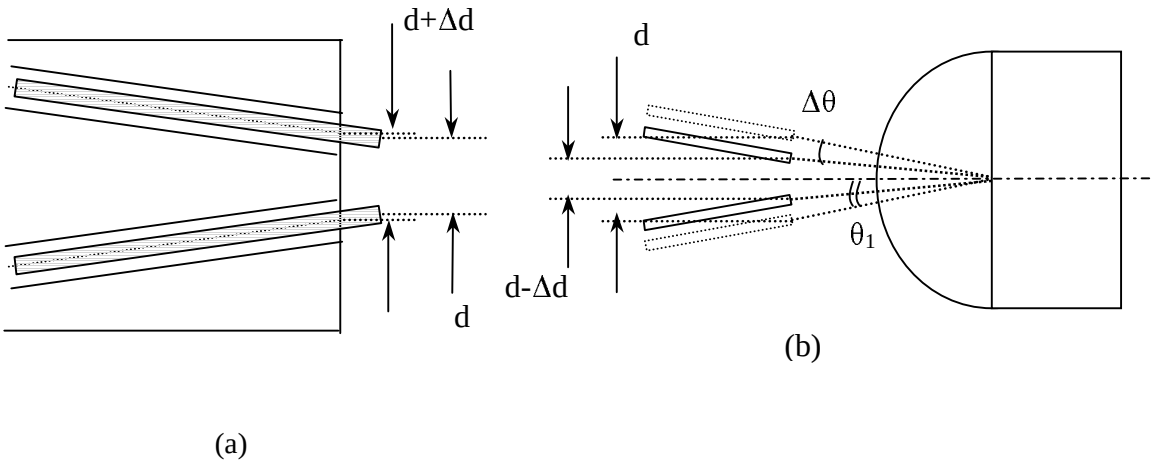

Fig. 9 Compensation of mechanical inaccuracy and misalignments in v-groove assembly. (a) Compensation of mechanical inaccuracy. (b) Angular mismatch for SMF case: The ideal fiber position are shaded, at a separation *d*. The actual separation is *d-⊿d*, Which is equivalent to an angular deviation of *⊿θ* from the ideal angle θ_1. Note unlike for TEC fibers, the single-mode fibers are not sensitive to angular misalignments. *Figures are not drawn to scale.*

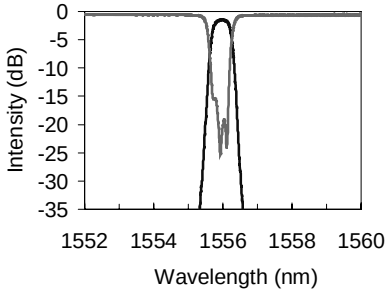

Fig. 10 Measured spectra of a 100-GHz ball-lens based OADM.